FEA-based Geometrical Modification of Switched Reluctance Motor for Radial Force Reduction

Rani S and Jayapragash R[*]

(School of Electrical Engineering, Vellore Institute of Technology, Chennai 600 127, India)

Abstract: Switched reluctance motors (SRMs) are becoming increasingly popular in the automotive sector owing to their robust design. Moreover, SRMs are preferred particularly for EV applications owing to their fault tolerance, magnet-free structure, and high power/torque density. The main concerns of SRM compared to other machines include torque ripple and vibration. The primary cause of vibration is the radial force created by the SRM. A geometry-based modification of the SRM to reduce the radial force without significantly changing the average torque produced is proposed. The primary goal is to design a 4-phase, 8/6 SRM with a lower radial force. Two possible geometrical alterations are proposed: one with square windows and the other with circular holes on the rotor core. The windows are sized and positioned to avoid flux saturation. General criteria are developed for the optimal window size and placement. Finite element analysis (FEA) modelling of the SRM is used to validate its performance. The FEA results are compared with the performance parameters obtained using the analytical method. Utilizes the multiphysics design tool ANSYS to obtain the natural frequencies and associated deformations through modal analysis. Compared to the conventional geometry, the radial force is significantly reduced by providing windows.

Keywords: 8/6 SRM, radial force, modal analysis, FEA analysis, natural frequencies, SRM with windows

1 Introduction

The popularity of switched reluctance motors (SRMs) is increasing owing to their ease of production, fault tolerance, and magnet-free structure. Although SRMs offer significantly more benefits than other electrical machines, their application in automobiles is restricted because of torque ripples and vibrations. In the SRM, an electromagnetic force is generated by exciting the coils on the stator poles that are opposite to one another. This force can be classified as tangential (longitudinal) and radial. The longitudinal force produces torque, while the radial force is responsible for torque ripple and vibration. Numerous studies to reduce the radial force in SRM have been proposed. Desai et al. [1] proposed an SRM with more rotor poles than stator poles. Under non-saturated conditions, this type generates less torque ripple. However, the torque ripple is more significant under saturated conditions than in conventional SRMs. Generally, a larger number of poles reduces the overloading capacity of the motor and requires complex converters and controller units [2-3]. One way to reduce torque ripple is to skew the stator and rotor [4-5]. A skewed geometry reduces the radial and tangential forces, and decreases the average torque. The geometry will become more sophisticated while skewing. Gundogmus et al. [6] proposed an SRM with rectangular holes in the stator and the rotor. Even though the radial force decreased, the maximum and average torques also decrease with the window size. Ref. [7] suggested a geometrical modification of the stator pole bridges to reduce the radial force. The bridges on the stator increases the weight of the motor. An SRM with circular perforations on the rotor poles was proposed in Ref. [8]. However, flux saturation occurred at the pole tips owing to the rotor pole holes. Ref. [9] proposed a double stator SRM for a radial force reduction. However, the proposed topology complicates the geometry. In-wheel motors (IWMs) [10] offer another e-powertrain option. Zhu et al. [11] proposed an improved IWSRM using a multiobjective optimization

Manuscript received March 6, 2023; revised September 11, 2023; accepted September 27, 2023. Date of publication March 31, 2024; date of current version January 11, 2024.
* Corresponding Author, E-mail: jayapragashr@vit.ac.in
Digital Object Identifier: 10.23919/CJEE.2024.000049

technique for EV applications. The design of an IWSRM for EV applications was presented in Ref. [12]. Unsprung mass is a considerable problem in IWMs. IWMs are exposed to road debris, dust, water, and mud, which decrease their torque compared with conventional motors.

This study proposes two distinct geometry-based modifications to reduce radial force. Circular holes and square windows are added to the conventional SRM in the axial direction. The main achievement of this study is that by adding windows to the rotor, the radial force is diminished without reducing the average torque. The primary challenge is the use of sizing and positioning windows to prevent flux crowding in the core. Although SRMs with various window structures are available in the literature, a universal criterion for deciding the position to place windows has not been established. To solve this problem, new criteria are proposed in this study. The article is structured as follows: Section 2 provides an FEA analysis of a conventional SRM. Section 3 includes both the geometrical modifications and corresponding FEA analysis. The estimation of the weight of the motor is presented in Section 4. Section 5 presents a comprehensive discussion of the findings. Section 6 presents a modal analysis. Finally, Section 7 provides a summary and concludes the paper.

2 Finite element analysis of conventional 8/6 SRM

The geometric parameters of the 4-phase 8/6 SRM were obtained by solving a fundamental output equation [13]. Tab. 1 lists the fundamental specifications of the geometrical design. In this study, the e-rikshaw was chosen as the application. The power requirements of the motor can be derived from the tractive force presented in previous works [14-15]. The geometric parameters of 8/6 SRM are listed in Tab. 2. M-19 steel was assigned to the rotor and stator portions of the geometry.

Tab. 1 Electrical specifications of 8/6 SRM

Parameter	Value
Output power P_{Kw}/kW	1
Motor speed N/(r/min)	3 000
Peak current I/A	20
Input voltage/V	72
Continuous torque T_D/(N • m)	3.18

Tab. 2 Geometrical parameters of 8/6 SRM

Parameter	Value
Rotor pole arc β_r/(°)	25
Stator pole arc β_s/(°)	23
Shaft diameter D_{sh}/mm	14
Outer diameter D_o/mm	120
Pole height (Rotor) h_r/mm	14.2
Pole height (Stator) h_s/mm	18.5
Stack length L_s/mm	120

The performance characteristics of the 4-phase 8/6 SRM were determined using FEA. The machine design tool Mag-Net was utilized for FEA modeling. Fig. 1 shows the wireframe and mesh patterns of a 4-phase 8/6 SRM. A static analysis was performed by exciting phase-A with varying current values. The flux linkage was at its maximum when the rotor was aligned and at it was at its lowest when the rotor was at the unaligned position. Fig. 2 illustrates the flux patterns for the same. The flux linkage characteristics for various current values and rotor positions are presented in Fig. 3. Fig. 4 shows the corresponding inductance profiles. Based on the inductance characteristics, the inductance at the unaligned rotor position was the smallest (5.031 mH) and remained constant regardless of the current value. The maximum aligned inductance varies with the current flowing through the windings. The static torque curve of the 4-phase 8/6 SRM is depicted in Fig. 5. The produced electromagnetic torque is a function of the current and the change in inductance caused by the rotor position, as shown in Eq. (1) [13]. A maximum torque of 12.781 N • m was generated by the model for a current of 20 A.

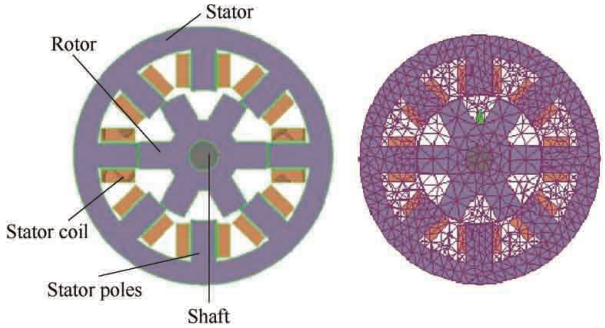

Fig. 1 Wireframe and meshed pattern of 4-phase 8/6 SRM

$$T_e = \frac{1}{2} i^2 \frac{\mathrm{d}L}{\mathrm{d}\theta} = \frac{1}{2} i^2 \frac{L_a}{\beta_s} \left(1 - \frac{L_u}{L_a} \right) \tag{1}$$

where $\frac{\mathrm{d}L}{\mathrm{d}\theta}$ indicates the change in inductance relative to the rotor position and L_u and L_a indicate the unaligned and aligned inductances, respectively.

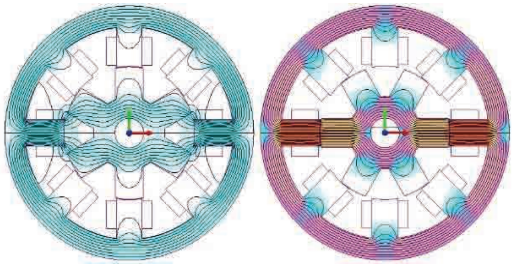

Fig. 2 Flux patterns of conventional 8/6 SRM at unaligned and aligned positions

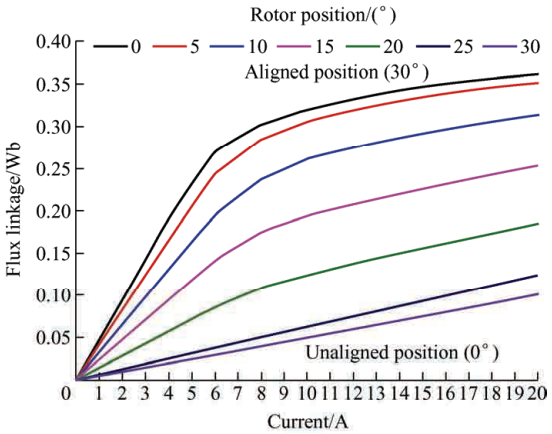

Fig. 3 Flux linkage plots of conventional 8/6 SRM

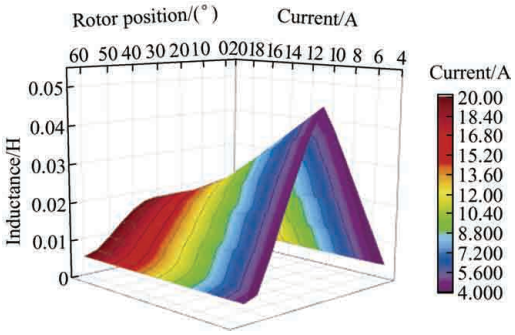

Fig. 4 Inductance characteristics of the conventional 8/6 SRM

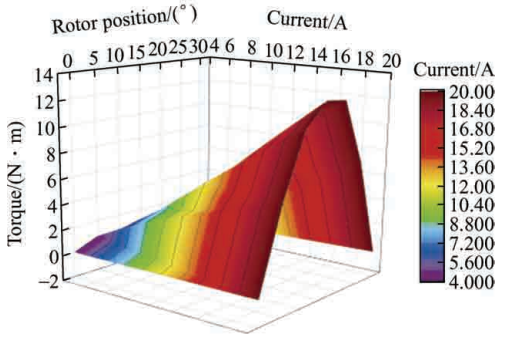

Fig. 5 Static torque characteristics of conventional 8/6 SRM

Transient analysis [14, 16] helps evaluate the performance characteristics over time. An asymmetric half-bridge converter powers the SRM, and the power circuit diagram is shown in Fig. 6. The conduction angle for this model was selected to be 20° for each phase. Fig. 7 depicts the voltage across the input side capacitor of the converter during the transient operation. The time profile of the flux linkage is shown in Fig. 8. Transient analysis was performed at 3 000 r/min. Figs. 9 and 10 show the current flowing through the coils and the generated transient torque, respectively. Based on the data given by the torque profile, this model can produce an average torque of 3.2 N • m continuously.

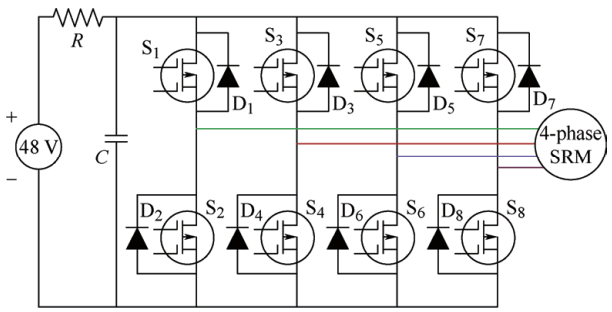

Fig. 6 4-phase asymmetric bridge converter of conventional 8/6 SRM

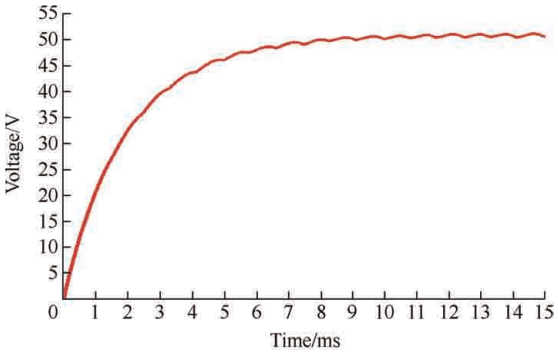

Fig. 7 Voltage across the input-side capacitor

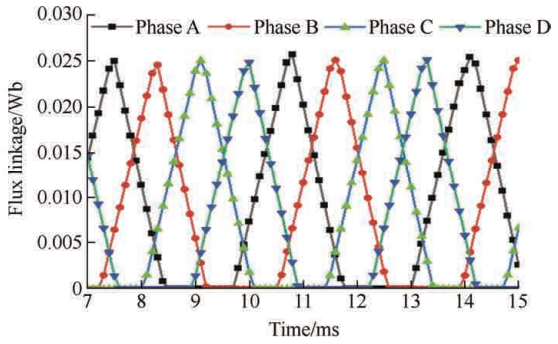

Fig. 8 Flux linkage plots of conventional 8/6 SRM

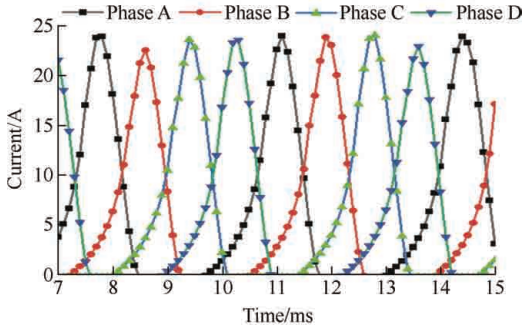

Fig. 9 Current flowing through the winding

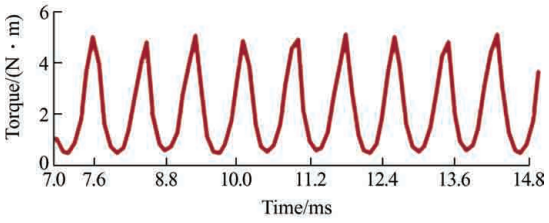

Fig. 10 Transient torque characteristics of 8/6 SRM

The air gap force was calculated using Maxwell's stress-tensor method, expressed as Eqs. (2) and (3), where B_T denotes the flux density, μ_0 indicates the permeability of free space, and $\boldsymbol{n}$ represents the normal unit vector. The total surface force is given by Eq. (3). The total force can be split into two components: the tangential force (F_{tn}) and radial force (F_{rd}), using Eqs. (4) and (5) [13-14]. B_{rd} and B_{tn} represent the radial and tangential flux density components in the air gap, respectively.

$$T_e = \frac{1}{\mu_0}\left[\left(B_T \cdot \boldsymbol{n}\right)B_T - \frac{1}{2}\Delta B_T^2 \cdot \boldsymbol{n}\right] \tag{2}$$

$$F_e = \iint T_e \mathrm{d}S \tag{3}$$

$$F_{tn} = \iint \frac{1}{\mu_0}\left(B_T \cdot \boldsymbol{n}\right)B_T \mathrm{d}S = \frac{1}{\mu_0}\iint B_{rd} \cdot B_{tn} \mathrm{d}S \tag{4}$$

$$F_{rd} = \iint \frac{1}{2\mu_0}\left(\Delta B_T^2 \cdot \boldsymbol{n}\right)\mathrm{d}S = \frac{1}{2\mu_0}\iint \left(B_{rd}^2 - B_{tn}^2\right)\mathrm{d}S \tag{5}$$

Fig. 11 shows the radial force of a 4-phase 8/6 SRM. The maximum radial force corresponding to a motor speed of 3 000 r/min is 26.12 N.

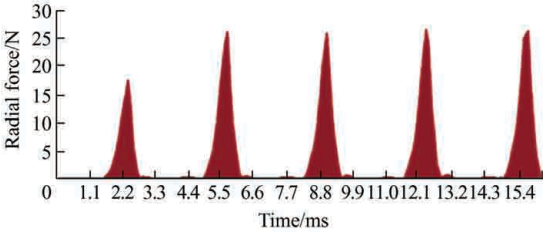

Fig. 11 Radial force obtained for conventional SRM

3 Structural modification of 8/6 SRM

Structural modifications were performed to reduce the radial force. The rotor geometry was altered by providing square and circular holes (windows) on the rotor core. The flux lines crossing per unit area differed among the materials. In the proposed method, the medium (material) was changed from M-19 steel (core) to air (windows) and M-19 steel again. As air has a higher reluctance than steel, windows obstruct the smooth flow of radial flux components. Owing to the decrease in the radial flux components, the radial force decreases when windows are provided. FEA was used to validate the performance of the modified geometries.

3.1 SRM with square windows on the rotor

The conventional SRM geometry was altered by adding square-shaped windows to the rotor along the longitudinal axis, as shown in Fig. 12. These windows have 4 mm sides on each side. The maximum possible square size was selected for the analysis. As the window size increased, the mass and mass moment of inertia of the motor decreased. However, the size is limited owing to the flux saturation on the rotor core. The flux saturation also varies with the core material. Determining the ideal window measurements and locations is the most challenging aspect of this design. The window size and placement criteria were developed to avoid flux saturation in the rotor cores. The following is a list of the proposed criteria.

$$d = \frac{1}{2}\left(D_{sh} + C_r\right) \tag{6}$$

$$W_s < \frac{C_r}{2} \tag{7}$$

$$W_s < W_{rp} \tag{8}$$

where d denotes the distance between the center of the hole and the motor shaft, D_{sh} indicates the shaft diameter, W_s denotes the side of the square window, W_{rp} indicates the rotor pole width, and C_r indicates the back iron thickness of the rotor.

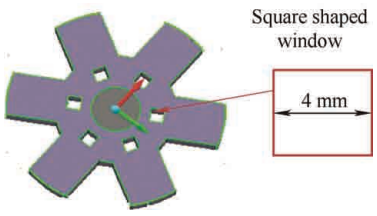

Fig. 12 Rotor modified with square windows

The performance characteristics were obtained from the FEA analysis. The flux linkage properties for various rotor positions and current levels are shown in Fig. 13.

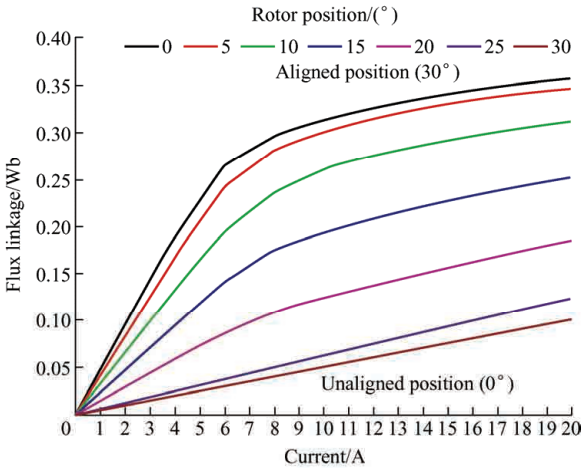

Fig. 13 Flux linkage characteristics of the SRM with square windows

Fig. 14 illustrates the inductance curve for various current values. The flux linkage at the unaligned position is minimal; hence, the inductance is also minimal at this position, 5.032 mH. The profile of the static torque is shown in Fig. 15. The maximum amount of torque produced by this model with a current of 20 A is 12.734 N • m.

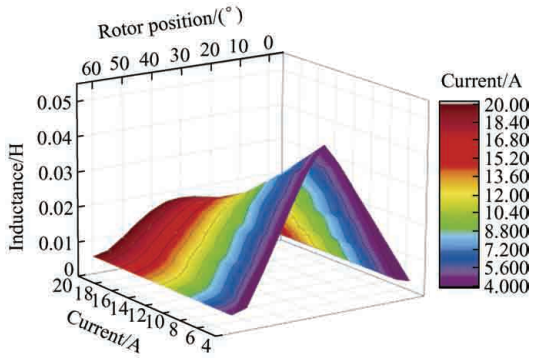

Fig. 14 Inductance plots of the SRM with square windows

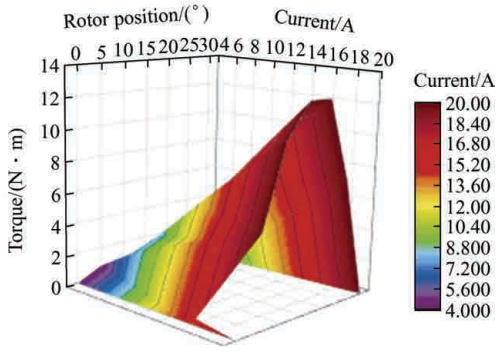

Fig. 15 Static torque characteristics of the SRM with square windows

Fig. 16 shows the current flowing through the coils. The flux linkage characteristics with respect to time are shown in Fig. 17. Fig. 18 presents the transient torques' characteristics. Compared with the traditional SRM, the radial force of the SRM with square windows is significantly reduced, 0.07 N, as shown in Fig. 19.

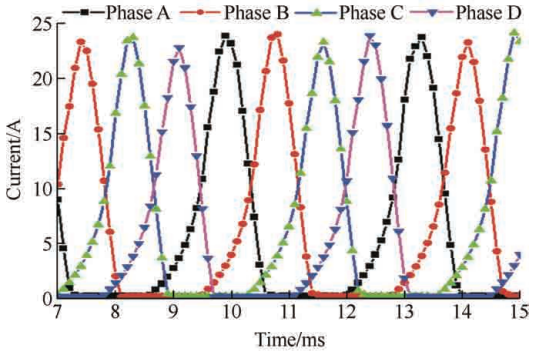

Fig. 16 Current flowing through the winding of SRM with square-shaped holes

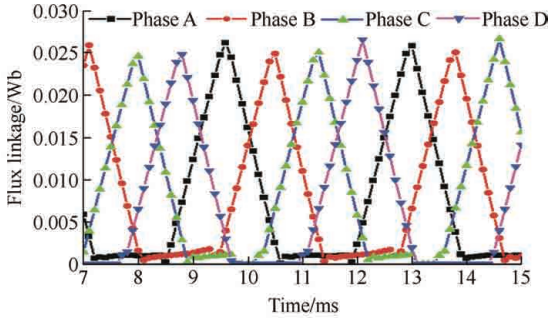

Fig. 17 Flux linkage of SRM with square-shaped windows

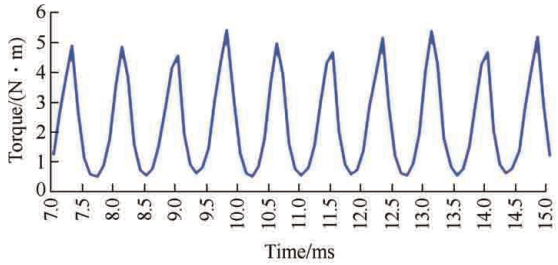

Fig. 18 Transient torque characteristics of SRM with square-shaped window

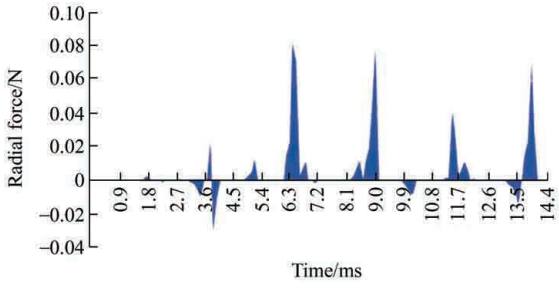

Fig. 19 Radial force plot of the SRM with square windows

3.2 SRM with circular/round holes on the rotor

The addition of circular holes to the rotor in the

longitudinal direction, as shown in Fig. 20, modifies the geometry of the conventional SRM. Six holes with radii of 3 mm were located within the rotor core. As there exists six rotor poles, six holes were created to ensure symmetry. The maximum possible hole size without flux saturation in the core was selected. To determine the appropriate size and location of the holes, the following general criteria are proposed [10].

$$d = \frac{1}{2}\left(D_{sh} + C_r\right) \tag{9}$$

$$D_h < \frac{C_r}{2} \tag{10}$$

$$D_h < W_{rp} \tag{11}$$

where d denotes the distance between the centers of the hole and the motor, D_h indicates the hole diameter.

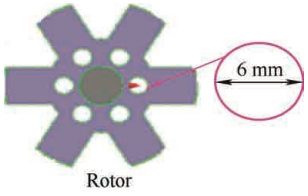

Fig. 20 Rotor modification with circular holes

Fig. 21 depicts the flux patterns for the same model in the aligned and unaligned positions. The flux linkage properties at different rotor angles and inductance profiles are depicted in Figs. 22 and 23, respectively. The unaligned inductance is 5.034 mH.

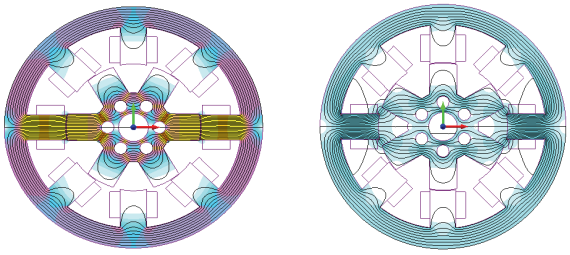

Fig. 21 Flux pattern of 8/6 SRM with circular holes at the aligned and unaligned position

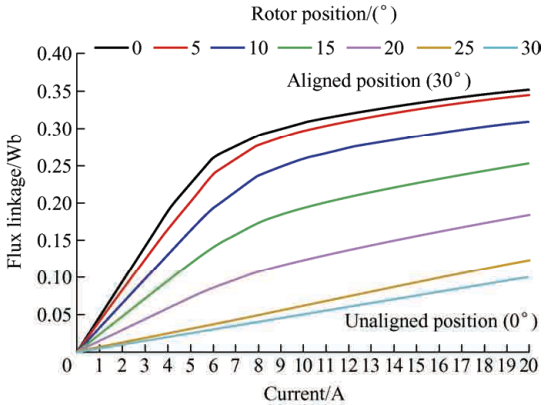

Fig. 22 Flux linkage characteristics of SRM with circular holes

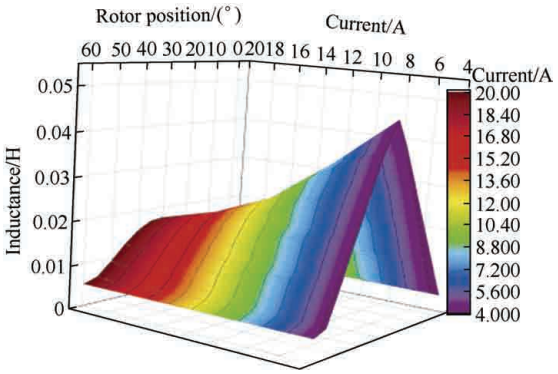

Fig. 23 Inductance profile of the SRM with circular holes

The static torque profile is shown in Fig. 24. A current of 20 A produced a maximum torque of 12.684 N • m. The current flowing through the coils is shown in Fig. 25. Figs. 26 and 27 show the flux linkage and transient torque characteristics of the model, respectively. Fig. 28 illustrates the radial force, which dropped to 0.015 N; the radial force in this topology is much less than that in the conventional topology.

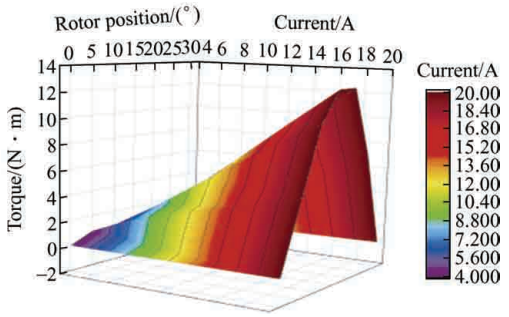

Fig. 24 Static torque profile of SRM with circular holes

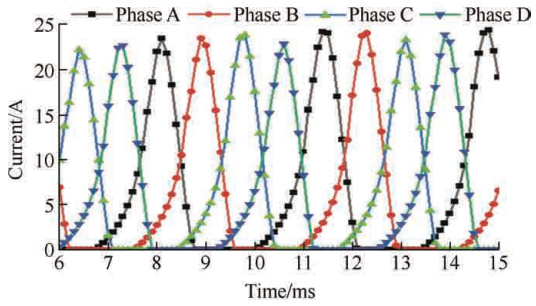

Fig. 25 Current flowing through the winding of SRM with circular holes

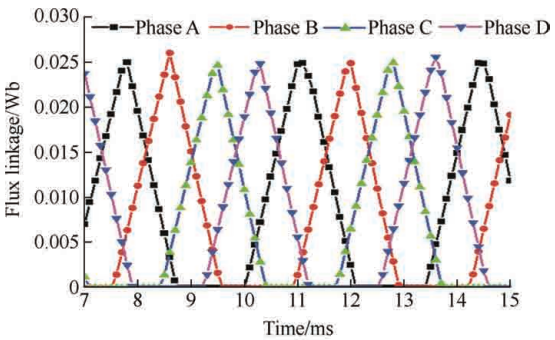

Fig. 26 Flux linkage of SRM with circular holes

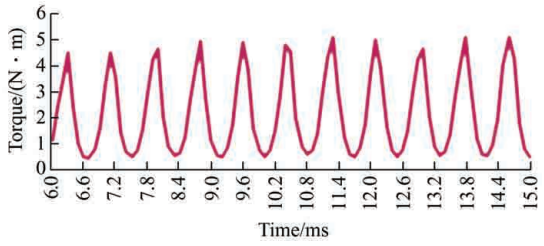

Fig. 27 Transient torque characteristics of SRM with circular holes

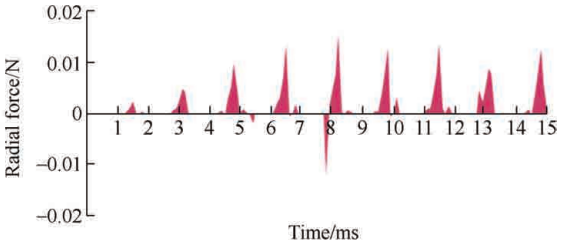

Fig. 28 Radial force of SRM with circular holes

3.3 Sizing of holes

From the FEA analysis, the SRM with circular holes produced the minimum radial force. Therefore, the optimal hole selection was performed using the static FEA method. The radius of the holes varied from 2 mm to 4 mm, and the performance was compared with that of a conventional motor. The flux linkage and torque for a current of 20 A at various rotor positions were obtained using FEA. Fig. 29 shows the flux linkage characteristics of the motor with holes in the rotor core. The flux linkage decreased with an increase in the window size.

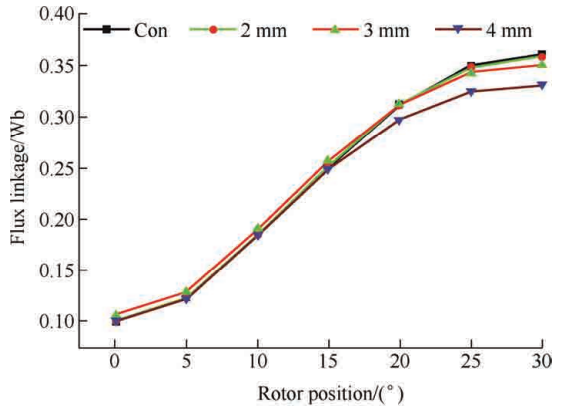

Fig. 29 Flux linkage characteristics for various hole sizes

The torque characteristics at various rotor positions and rated speeds are presented in Fig. 30. As the flux linkage decreases, the average torque also decreases, although the maximum torque remains constant. Therefore, holes with a diameter of 6 mm are preferable for this geometry to reduce the radial force without significantly reducing the average torque. The flux linkage at the aligned position was reduced to 99.4%, 97.38%, and 91.97%, respectively, for the SRM with holes of 2 mm, 3 mm and 4 mm radius compared to the conventional motor. The reduction in the flux linkage reduces the average torque, even though the maximum torque remains almost constant. The average torque is reduced to 99.16% (7.11 N • m), 96.23% (6.90 N • m), and 87.16% (6.25 N • m), respectively, for SRM with holes of 2 mm, 3 mm, and 4 mm radii compared to the conventional motor (7.17 N •m). Flux saturation increases with the window size. Therefore, there should be a compromise between the mass, radial force, and average torque of the motor. Therefore, a hole with a radius of 3 mm was selected for this geometry. The same procedure was followed to select the size of the square windows.

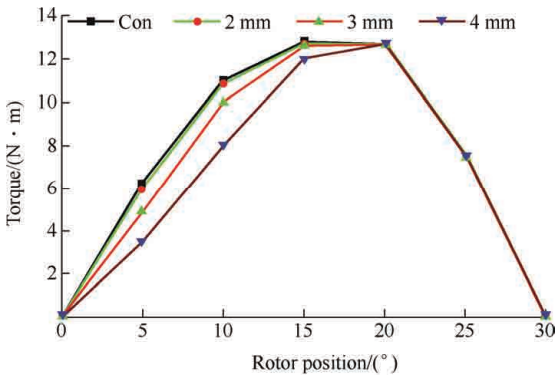

Fig. 30 Static torque characteristics of motors with various hole sizes in the rotor

4 Calculation of mass

The mass of the motor is calculated analytically as follows: M19 steel [17-18] has a mass density (ρ) of 7 650 kg/m^3. The mass of the stator pole (m_{sp}) is estimated by [14]

$$m_{sp} = h_s L_s \frac{D}{2} \beta_s \rho \tag{12}$$

The mass of the stator core (m_{sy}) was estimated as

$$m_{sy} = \pi L_s \left(S_{or}^2 - S_{ir}^2 \right) \rho \tag{13}$$

where S_{or} and S_{ir} are the outer and inner radii of the stator yoke, respectively. The same method is used to estimate the mass of the rotor pole (m_{rp}).

$$m_{rp} = h_r L_s \left(\frac{D}{2} - g \right) \beta_r \rho \tag{14}$$

The rotor core mass (m_{ry}) is estimated as

$$m_{ry} = \pi L_s \left(r_{or}^2 - r_{ir}^2 \right) \rho \tag{15}$$

where r_{or} and r_{ir} are the outer and inner radii of the rotor yoke, respectively. The total mass of the traditional model was estimated as 6.65 kg using the above equations. Similarly, the mass of the modified models was computed by reducing the volume of windows in the traditional model.

Tab. 3 lists the masses and mass moments of inertia for the conventional and modified geometries. These findings indicate that the shape of the windows significantly minimizes the mass and mass moment of inertia of the rotor. Only the rotor mass is tabulated in Tab. 3 because the alteration is limited to the rotor component.

Tab. 3 Comparison of mass and mass moment of inertia

Geometry	Rotor mass (FEA)/kg	Rotor mass (Analytical)/kg	Mass moment of inertia/(kg • m^2)
Conventional SRM	1.768 8	1.756 9	0.000 761
SRM with circular holes	1.618 8	1.601 1	0.000 739
SRM with square-windows	1.678 8	1.668 7	0.000 749

5 Results comparison and discussion

Performance metrics such as torque, aligned inductance, unaligned inductance, mass, mass moment of inertia, and radial force are compared in Tab. 4. The minimum inductance was slightly altered because of the windows on the core. The average torque may remain constant even after a geometric change. Fig. 31 shows a static torque comparison developed for a current of 20 A.

Tab. 4 Comparison of performance parameters

Parameter	Conventional SRM	Rotor with circular holes	Rotor with square-shaped windows
Aligned inductance/mH	18.054	17.562	17.813
Unaligned inductance/mH	5.031	5.034	5.032
Max. developed torque/(N • m)	12.78	12.68	12.73
Mass of rotor/kg	1.756 9	1.601 1	1.668 7
Mass moment of inertia/(kg • m^2)	0.000 761	0.000 739	0.000 749
Radial force/N	26.12	0.015	0.07
Torque ripple/(N • m)	3.78	3.28	3.63
Torque ripple(%)	29.58	25.86	28.53
Average torque/(N • m)	7.17	6.904	7.05

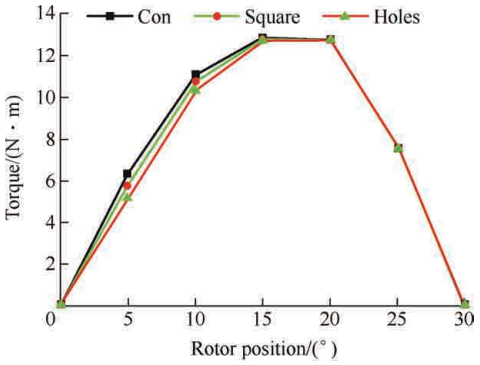

Fig. 31 Comparison of static torque characteristics

Static FEA shows no appreciable difference between the maximum torque produced by the modified models and the conventional SRM. As shown in Fig. 32, the geometric modification significantly lowers the radial force. The motor mass and moment of inertia decrease when the windows were supplied. As this study focuses on the application of electric vehicles, the mass and mass moment of inertia are regarded as two of the most critical variables. Vehicles frequently accelerate and decelerate based on the driving cycle. Therefore, for a vehicle to operate smoothly, its mass and moment of inertia should be minimized. The rotor core with circular perforations reduces the rotor mass by 156 g. In contrast, a rotor with a square window reduced the mass by 88 g. The static torque characteristics determine the torque ripple using Eq. (16). The torque ripple was reduced by 1.047% and 3.722%, respectively, by adding square windows and circular holes to the rotor. For e-rickshaw applications, SRMs

with circular holes are favored owing to their low mass, moment of inertia, and torque ripple, although SRMs with square-shaped windows on the rotor provide almost the same maximum torque as conventional SRMs.

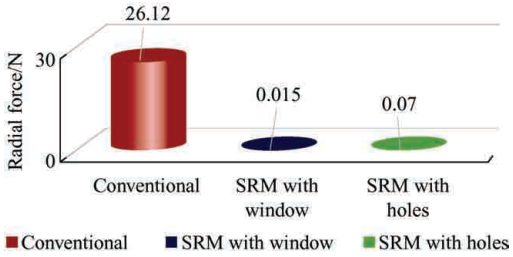

Fig. 32 Comparison of radial force

$$\%\ \text{Torque ripple} = \frac{T_{\max} - T_{\min}}{T_{\max}} \times 100 \tag{16}$$

where $T_{\max}$ and $T_{\min}$ denote the maximum and minimum torque values obtained from the static torque characteristics, respectively.

6 Modal analysis

Using the multiphysics design tool ANSYS, a modal analysis was performed to identify the natural frequencies of the geometry. The mechanical properties of the core material, M-19 steel, employed in the analysis are Young's modulus (E)=2.07 GPa, Poisson's ratio (υ)=0.3, and material density (ρ)=7 650 kg/m^3. The excitation frequency of the SRM was determined using Eq. (17) [19-22].

$$f_0 = \frac{NP_r}{60}\left(\frac{P_s}{2}\right) \tag{17}$$

where P_r and P_s represent the numbers of rotor and stator poles, respectively. At 3 000 r/min, the excitation frequency of 8/6 SRM was 1 200 Hz. The differential equation for motor motion can be expressed in matrix form using the stiffness approach, as shown in Eq. (18).

$$\boldsymbol{M}_m\{\ddot{\boldsymbol{X}}\} + \boldsymbol{C}_m\{\dot{\boldsymbol{X}}\} + \boldsymbol{K}_m\{\boldsymbol{X}\} = \boldsymbol{F}_m(t) \tag{18}$$

where $\boldsymbol{M}_m$ indicates the mass matrix, $\boldsymbol{C}_m$ represents the damping matrix, $\boldsymbol{K}_m$ represents the stiffness matrix, $\ddot{\boldsymbol{X}}$ represents the acceleration vector, $\dot{\boldsymbol{X}}$ represents the velocity vector, $\boldsymbol{X}$ represents the displacement vector, and $\boldsymbol{F}_m(t)$ represents the force vector. Generally, damping is discarded when determining the natural frequency. Let $\boldsymbol{F}_m$ = {0} and the eigenvalue equation of the undamped modal analysis of the model is [19]

$$\boldsymbol{K}_m - \omega^2 \boldsymbol{M}_m\{\boldsymbol{X}\} = \{0\} \tag{19}$$

By resolving ω and {$\boldsymbol{X}$} of Eqs. (18) and (19), the natural frequencies and modal mode shapes can be found in Eq. (19) [17-22].

Fig. 33 presents the modal analysis results for the conventional SRM rotor. Because this is a free-body vibration, the first six modes exhibited lower frequency values. Therefore, 14 modes were considered in this study. The natural frequencies and corresponding deformations from the 7th to 14th modes are displayed. The natural frequencies and corresponding total deformations of the modified geometries are shown in Figs. 34 and 35, respectively. Fig. 34 shows a rotor with square windows. Fig. 35 shows a rotor with circular windows in its core. The total deformation of the modified rotor structures was less than that of the conventional SRM. Tab. 5 lists the natural frequencies and corresponding total deformations of all three models obtained from the modal analysis.

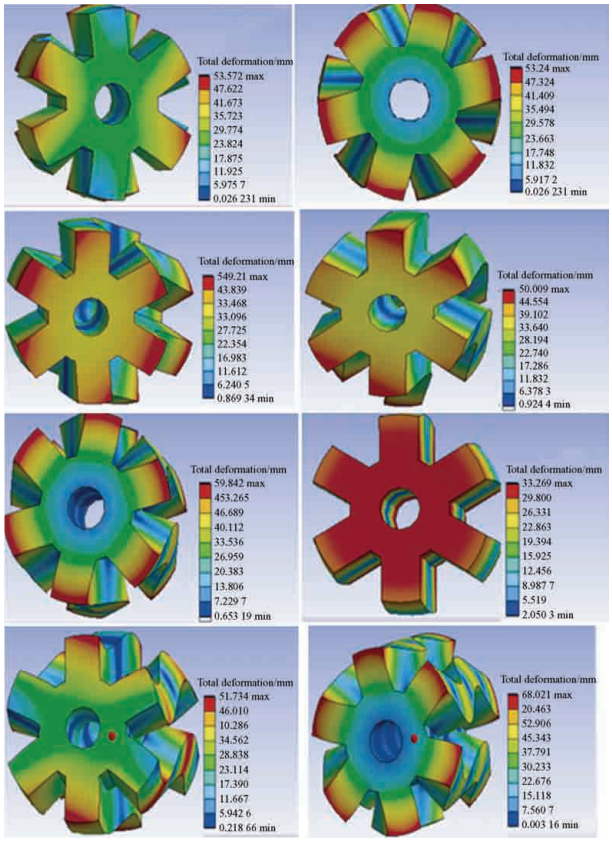

Fig. 33 Natural frequency and mode shapes of conventional SRM

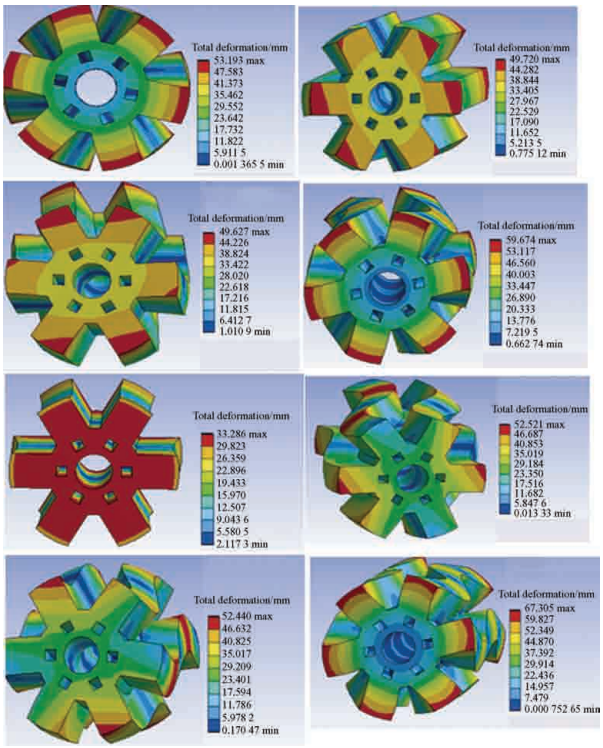

Fig. 34 Natural frequency and mode shapes of SRM with square windows

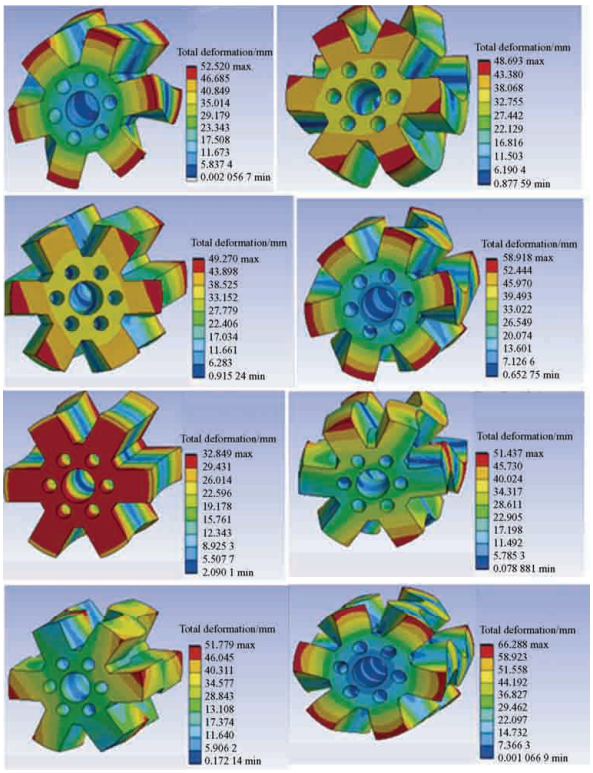

Fig. 35 Natural frequency and mode shapes of SRM with circular holes

Tab. 5 Comparison of natural frequencies and the corresponding maximum deformation

Mode	Conventional SRM rotor		With square shaped window		With circular holes	
	Frequency/Hz	Max. deformation	Frequency/Hz	Max. deformation	Frequency/Hz	Max. deformation
1	0	22.588	0	22.588	0	22.588
2	0	22.588	0	22.588	0	22.588
3	6.46×10^{-3}	22.588	3.27×10^{-3}	22.588	1.08×10^{-2}	22.588
4	10.121	41.098	4.356 9	41.363	4.778 8	40.797
5	10.87	41.352	4.658 5	41.011	5.539 4	40.836
6	41.884	35.758	12.784	35.758	19.55	32.298
7	7 798.4	53.24	7 786.1	53.193	7 681.5	52.52
8	12 074	49.21	12 075	49.72	11 918	48.693
9	12 079	50.009	12 075	49.624 7	11 920	49.27
10	15 843	59.842	15 819	59.674	15 607	58.918
11	21 003	33.458	21 002	33.286	20 733	32.849
12	21 273	53.572	21 266	52.52	20 994	51.437
13	21 299	51.734	21 271	52.44	21 002	51.779
14	24 404	68.012	24 371	67.305	24 045	66.288

The deformation was reduced when the windows were inserted into the rotor core. For instance, for mode 7, the maximum deformation is 53.24 mm for the conventional motor. The maximum deformation on the rotor reduced to 52.52 mm and 53.193 mm for the rotor with circular holes and square windows, respectively. The maximum deformation of the rotor with circular holes was reduced to 98.65% of that of a conventional motor.

7 Conclusions

This study investigated the efficiency of providing

windows in the rotor core to reduce the radial force. The performance of different window shapes in the rotor core was studied. General criteria were developed for the positioning and selection of the window size in the rotor core without causing flux saturation. For all three models, a modal analysis was performed to compare the total deformation at various natural frequencies during free vibration. Statistics indicate that the excitation frequency does not coincide with the natural frequencies. Motor vibration increases if the natural and excitation frequencies are equal. Upon inserting the windows in the rotor core, the overall deformation of the structure was significantly reduced compared to that of the conventional SRM topology.

The improved geometries lowered the radial force from 26.12 N to 0.015 N and 0.07 N. Owing to the existence of windows, mass and moment of inertia are decreased. The rotor mass was reduced to 94.9% (1.678 8 kg) and 91.5% (1.618 8 kg) for the SRM with square and circular holes, respectively, compared to the conventional rotor (1.768 8 kg). The most important contribution of this research is the reduction in radial force without appreciable changes in the average and maximum torques. The average torques obtained are 7.17 N • m, 7.05 N • m, and 6.904 N • m for the conventional motor, with square and circular windows, respectively. This variation in the torque can be attributed to the slight variation in the flux linkage when the windows were inserted into the core. The maximum torque remained almost constant even after the geometrical modification. The maximum torques for the conventional motor with square and circular windows were 12.78 N • m, 12.73 N • m, and 12.68 N • m, respectively.

Moreover, the torque ripple is reduced by 3.721 74% with circular holes in the rotor structure. The mass, mass moment of inertia, radial force, and percentage torque ripple are the critical variables for the final selection. Consequently, an SRMs with round windows on the rotor core is proposed for EV applications.

References

[1] P C Desai, M Krishnamurthy, N Schofield, et al. Novel switched reluctance machine configuration with higher number of rotor poles than stator poles: Concept to implementation. *IEEE Transactions on Industrial Electronics*, 2010, 57(2): 649-659.

[2] H Cheng, H Chen, Z Yang. Design indicators and structure optimization of switched reluctance machines for electric vehicles. *IET Electric Power Applications*, 2015, 9(4): 319-331.

[3] P V Raghavan. Design of switched reluctance motor and development of a universal controller for switched reluctance and permanent brushless DC motor drives. Virginia: Virginia Polytechnic Institute and State University, 2004.

[4] H Yang, Y Lim, H Kim. Acoustic noise vibration reduction of a single-phase SRM using skewed stator and rotor. *IEEE Transactions on Industrial Electronics*, 2013*,* 60(10): 4292-4300.

[5] C Gan, J Wu, M Shen, et al. Investigation of skewing effects on the vibration reduction of three-phase switched reluctance motors. *IEEE Transactions on Magnetics*, 2015, 51(9): 1-9.

[6] O Gundogmus, M Elamin, Y Yasa, et al. Acoustic noise mitigation of switched reluctance machines with windows on stator and rotor poles. *IEEE Transactions on Industry Applications*, 2020, 56(4): 3719-3730.

[7] G F Lukman, X S Nguyen, K I Jeong, et al. Design and performance analysis of switched reluctance motor with inner holes to reduce radial force. *IEEE Energy Conversion Congress and Exposition (ECCE)*, 11-15 October, Detroit, MI, USA. IEEE, 2020: 4697-4702.

[8] T D Gupta, K Chaudhary, R M Elavarasan, et al. Design modification in single-tooth winding double stator switched reluctance motor for torque ripple mitigation. *IEEE Access*, 2021, 9: 19078-19096.

[9] S Das, O Gundogmus, Y Sozer, et al. Wide speed range noise and vibration mitigation in switched reluctance machines with stator pole bridges. *IEEE Transactions on Power Electronics*, 2021, 36(8): 9300-9311.

[10] G Nalinashini, V Tamilselvi. Experimental investigation of modified in-wheel switched reluctance motor with reduced torque ripple for electric vehicles. *Electrical Engineering*, 2021, 103: 2837-2845.

[11] Y Zhu, C Yang, Y Yue, et al. Design and optimization of an in-wheel-switched reluctance motor for electric vehicles. *IET Intelligent Transport Systems*, 2019, 13(1): 175-182.

[12] Z Omaç, M Polat, E Öksüztepe, et al. Design, analysis,

and control of in-wheel switched reluctance motor for electric vehicles. *Electrical Engineering*, 2018, 100(2): 865-876.

[13] R Krishnan. Switched reluctance motor drives: Modeling, simulation, analysis, design, and applications. Boca Raton: CRC Press, 2001.

[14] S Rani, R Jayapragash. Radial force reduction of switched reluctance motor for EV application. *2022 IEEE International Conference on Signal Processing, Informatics, Communication and Energy Systems* (*SPICES*), 2022: 470-475.

[15] S Rani, R Jayapragash. Design of SRM-based powertrain for e-rickshaw application. *2022 International Virtual Conference on Power Engineering Computing and Control: Developments in Electric Vehicles and Energy Sector for Sustainable Future (PECCON)*, 2022: 1-6.

[16] R Jayapragash, C Chellamuthu. Development of analytical models for switched reluctance machine and their validation. *Journal of Electrical Engineering and Technology*, 2015, 10(3): 990-1001.

[17] M Elamin, Y Yasa, Y Sozer, et al. Effects of windows in stator and rotor poles of switched reluctance motors in reducing noise and vibration. *IEEE International Electric Machines and Drives Conference (IEMDC)*, 21-24 May, Miami, FL, USA. IEEE, 2017: 1-6.

[18] C Gan, J Wu, Q Sun, et al. A review on machine topologies and control techniques for low noise switched reluctance motors in electric vehicle applications. *IEEE Access*, 2018, 6: 31430-31443.

[19] Y H Huang, C Chen, Y Yuan, et al. Analysis of electromagnetic vibration and noise characteristics of bearingless switched reluctance motor. *Progress in Electromagnetics Research M*, 2019, 85: 83-94.

[20] H Simin, A B Yousef. Noise reduction in switched reluctance motor by modifying the structures. *IET Electric Power Applications*, 2020, 14(14): 2863-2872.

[21] M Chris, M A Masrur. Hybrid electric vehicles principles and applications with practical perspectives. 2nd ed. NJ: Wiley, 2018.

[22] K Nakata, K Hiramoto, M Sanada, et al. Noise reduction for switched reluctance motor with a hole. *Proceedings of the Power Conversion Conference-Osaka*, 02-05 April, 2002, Osaka, Japan. IEEE, 2002, 3: 971-976.

Rani S (IEEE Member) has a Bachelor's degree in Electrical Engineering (AMIE) from the Institution of Engineers, India (2009). She graduated from Visveswaraya Technological University, Belgaum, with a Master's degree in Computer Applications in Industrial Drives (2012). She worked as an Assistant Professor in the Electrical and Electronic Engineering Department at MEA Engineering College, Kerala, India. She is a Ph.D. candidate at the School of Electrical Engineering, Vellore Institute of Technology, Chennai, India. Powertrain designs for EVs, power electronics, and special machines are some of the areas of interests.

Jayapragash R obtained his Bachelor's degree in Electrical Engineering (AMIE) from the Institute of Engineers, India (2004). He obtained his Master's degree in Power Electronics and Driving from Anna University in 2007. He received his Ph.D. from Anna University, Chennai for the Thesis titled "Development of analytical models and battery energy storage system for wind-powered switched reluctance generators". He has more than 7 years of work experience in the industry and 15 years of experience in the academic field. He is currently an Associate Professor in the School of Electrical Engineering at Vellore Institute of Technology Chennai, India. His research areas include machine design, battery management systems, and converter design for battery charging.